Chapter 1
Principles and Characteristics of Cold Plasma at Gas Phase and Gas-Liquid Phase

Jie Shen, Cheng Cheng, Zimu Xu, Yan Lan, Guohua Ni, and Siyuan Sui

Abstract Atmospheric pressure cold plasma is considered to have broad application prospects in different fields, such as plasma agriculture, food preservation, material preparation, and plasma medicine. This chapter presents the generation and characteristics of typical plasma sources that are suitable for different applications. Secondly, advances in plasma diagnostic techniques, plasma modeling, and simulations about gas phase, gas-liquid phase, and liquid phase are introduced in detail. The diagnostic results may offer the valid input to model calculations or validate the correctness of the simulation. Plasma simulation may provide some useful clues on the basic characteristics and kinetic reaction processes of plasma-liquid interaction. Thirdly, the formation mechanisms and physicochemical processes of reactive species coupled with the plasma liquid interaction are summarized. The main contents of this chapter will provide support for the efficient production of reactive species in gas phase and subsequently in liquid phase to meet the requirements of different low-temperature plasma applications.

Keywords Plasma agriculture · Food preservation · Material preparation · Plasma gas-liquid interaction · Gas-liquid phase products · Reactive species

1.1 Introduction

In recent years, healthy lifestyles and better diets have become the goal of people.

J. Shen (✉) · C. Cheng · Y. Lan · G. Ni · S. Sui
Institute of Plasma Physics, Chinese Academy of Sciences, Hefei, China

Anhui Province Key Laboratory of Medical Physics and Technology, Center of Medical Physics and Technology, Hefei Institutes of Physical Science, Chinese Academy of Sciences, Hefei, China
e-mail: shenjie@ipp.ac.cn

Z. Xu
School of Resources and Environmental Engineering, Hefei University of Technology, Hefei, China

T. Ding et al. (eds.), *Applications of Cold Plasma in Food Safety*,
https://doi.org/10.1007/978-981-16-1827-7_1

Fresh food products have received considerable attention (Liao et al. 2017). Fresh meat and poultry, eggs, vegetables, fruits, milk, and so on are the necessities of people's life, providing people with rich protein, vitamins, and cellulose. However, fresh food products are also the carrier of pathogenic microorganisms. One-third of food products are discarded due to postharvest improper operations and foodborne pathogens in the world (Bradford et al. 2018). The improvement of trade globalization and the increase of consumption will help to partly solve the waste problem of fresh food products postharvest. However, the increase of pathogen diversity on fresh food and the increased resistance of pathogens to the external environment are the main reason for foodborne illnesses (Murray et al. 2017).

The main pathogenic microorganisms isolated from fresh products include *Salmonella* and *Escherichia coli, Listeria monocytogenes,* and *Staphylococcus aureus*, which can survive in fresh and even frozen food for a long time, causing serious infection and even death (Ma et al. 2015). It can cause catastrophic harm to the health of consumers. Consequently, there is an urgent need to realize an effective sterilization method on fresh products that ensures food safety with minimal negative impacts on the sensory and nutritional qualities, and the taste of the food at the same time.

Researchers continue to innovate food processing from traditional "hot processing" to "cold processing" and have successively developed a series of nonthermal food processing technologies and equipment, such as ultra-high voltage, pulsed electric field, ultrasonic, and pulsed magnetic field (Jimenez-sanchez et al. 2017). Moreover, nonthermal plasma (low pressure and atmospheric pressure plasma) is a novel microbial inactivation technology and has great potential in offering an interesting alternative method. Though plasma is ubiquitous in the universe, the history of plasma sterilization is relatively short. The bactericidal effect of plasma is gradually recognized, since Menashi used argon plasma to inactivate bacteria on glass surface for the first time in 1968. Compared with low pressure plasma, atmospheric pressure plasma (APP) does not need expensive vacuum system and is easy to operate. Atmospheric pressure plasma has been widely researched over years in material surface engineering, environmental water pollution treatment, biomedicine, and food preservation (Shen et al. 2019; Khlyustova et al. 2019; Mir et al. 2016; Pan et al. 2019). Atmospheric pressure plasma generated in an open environment with different carrier gas is rich in charged particles, electric fields, ultraviolet (UV) photons, and reactive species, resulting in microbial inactivation (Lu et al. 2016a, b).

1.1.1 Application of APP in Food Industry

1.1.1.1 Application of APP in Food Sterilization and Preservation

Studies have confirmed that APP can sterilize bacteria, fungi, viruses associated with the processing and storage of poultry, eggs (Georgescu et al. 2017), meat products

(Bae et al. 2015), cereals and grains (Zahoranova et al. 2016; Suhem et al. 2013), fruit and vegetable products (Lacombe et al. 2015), and dairy products (Gurol et al. 2012), so as to achieve the purpose of long-term food storage and preservation.

1.1.1.2 Application of APP in Degradation of Mycotoxins and Pesticide Residues

The results showed that APP can effectively degrade mycotoxins (Hojnik et al. 2017), pesticide residues (Sarangapani et al. 2016), and other harmful chemicals in food.

1.1.1.3 Application of APP in Food Packaging

APP is widely used in the modification of food packaging materials (Pankaj et al. 2014). Cold plasma treatment can effectively inactivate microorganisms on the surface of the packaging materials, and the cold plasma treatment can also coat the surface of the packaging materials with high barrier film (blocking the penetration of oxygen and water vapor), effectively extending the sealing function of the packaging materials.

1.2 The Generation and Characteristics of Cold Plasma

1.2.1 Plasma and Its Classification

Plasma can be generated by enough external electric energy and is usually regarded as the fourth state of matter owing to its unique characteristic. Plasma is a partially or completely ionized gas composed of free electrons, ions, atoms, neutral molecules, and photons in metastable or excited state with electrically neutral nature (Misra et al. 2011).

Plasma is generally distinguished into low-temperature plasma ($T_e = 10^4$–10^5 K) and high-temperature plasma ($T_e = 10^6$–10^8 K) with different electron temperature (T_e). More specifically, low-temperature plasma can be subdivided into thermal plasma and nonthermal (cold) plasma according to different thermodynamic equilibrium state. It is necessary to decompose diatomic and ionize atoms to convert neutral gas into thermal plasma. The collision frequency is very high and allows energy transfer between the electrons and the ions species, leading to thermalization of different particle species to the final thermodynamic equilibrium. In this case, the electrons temperature (T_e) in thermal plasma is also the same as heavy ions temperature (ions and neutral molecules and atoms, T_i) and the gas temperature (T_g). The overall temperatures of thermal plasma can be in the order of 10^4 K and the ionization degree (number of ions over electrons and neutral particles) is very high.

In contrast, cold plasma is in local thermodynamic nonequilibrium state. The heavy ions temperature is kept at low temperature (300–500 K), whereas electrons temperature can reach as high as 10^4 K (Liao et al. 2017). The overall gas temperature can be as low as room temperature. Due to the high electron energy and low gas temperature, reactive oxygen species (ROS) and reactive nitrogen species (RNS) can be produced in gas phase according to different carrier gases, which is very suitable for quick sterilization and preservation in the food industry.

1.2.2 The Mechanism of Plasma Excitation

Electrical breakdown of gases means that a discharge channel is formed between the air gaps separated by two electrodes, when the applied voltage exceeds a certain critical voltage. It is generally accompanied by unique physical properties such as electricity, light flash, and sound and induces a series of chemical processes in gas phase. The main mechanism of the discharge occurrence and development is collision ionization and an electron attachment.

The acceleration of electrons in the electric field impacts and ionizes the gas molecules, producing many new electrons by excitation, which promotes the development and formation of a single electron avalanche (Fig. 1.1a). The single electron avalanche ionizes the surrounding gas and emits photoelectrons at the head of avalanche, which results in the development of secondary avalanches (Fig. 1.1b). The secondary avalanches concentrate at the head of main avalanche or at its sides under the action of main avalanche electric field. Therefore, avalanche formation and continuous development enhance the electric field in the discharge gap towards the cathode. With the increase of electric field strength, collision ionization also increases simultaneously, which promotes the continuous development of electron avalanche until the whole plasma discharge channel is filled. The plasma comprises positive ions left behind the previous electron avalanches and new electrons formed by subsequent avalanches. The expansion of the plasma discharge channel is caused by the continuous development of new avalanches (Gasanova 2013). As shown in

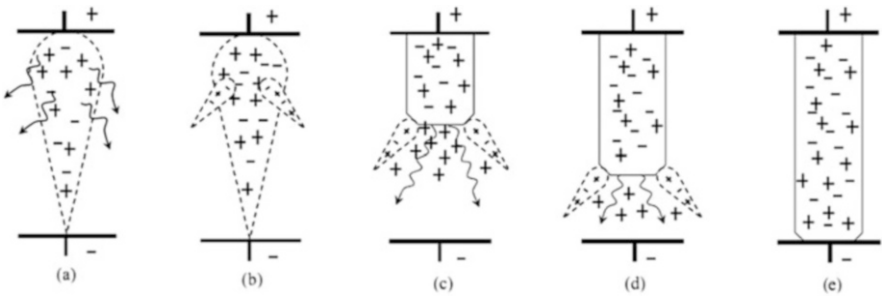

Fig. 1.1 Breakdown mechanism. (**a**) Growth of an electron avalanche; (**b**) generation of secondary avalanches; (**c**), (**d**) growth of a positive streamer; (**e**) the full electric breakdown (Gasanova 2013)

Figs. 1.1c, d, the partial plasma discharges generate between the discharge gaps. Fig. 1.1e shows the formation of full breakdown over the discharge gaps.

1.2.3 Chemical Reactions in Plasma Discharge

Atmospheric pressure nonthermal (cold) plasmas are excellent sources of ROS and RNS. When plasma discharge is excited, reactive species are generated through various collisions and energy exchange processes between electrons, atoms, and neutral gas molecules. Under the action of electric and electromagnetic fields, the free charges are accelerated and lead to abundant elastic or inelastic collisions. Elastic collisions generally redistribute kinetic energy, whereas the transferred energy is in a small proportion. By contrast, inelastic collisions can transfer energy up to 15 eV between different particles resulting in ionization, excitation, and dissociation reaction processes (Surowsky et al. 2015). The neutral gas molecules can interact with ions through charge transfer, ion recombination, associative detachment, transfer of excitation, or bond rearrangement reaction processes, and finally lead to the formation of stable species (Lieberman and Lichtenberg 1994; Braithwaite 2000). The direct ionization of ground-state atoms, gas molecules, and neutral free radicals by electron is the most significant ionization mechanism for atmospheric pressure cold plasmas. Through a series of energy transfer and excitation processes, plasma discharge is generated with rich ROS (such as OH radicals, atomic O, and O_3), RNS (NO radicals, atomic N), particles (Ar^+, N_2^+), electrons, and UV photons. The plasma will trigger rapid bactericidal effects on the food under the synergistic action of various active plasma agents. Plasma source, discharge mode, power, gas composition, and plasma interaction mode will affect the physical characteristics of plasma, such as electron density, electron temperature, and thus the composition and content of reactive species in gas phase and their final biological effects.

1.2.4 Various Atmospheric Plasma Sources

Atmospheric pressure cold plasma sources (plasma generation system) generally include suitable active power source, special electrode configurations, and a carrier gas system. The cold plasmas can be generated by applying electrical energy to the neutral gas (such as air, oxygen, nitrogen, helium, argon, or their admixtures). The cold plasmas are very efficient sources of reactive species, such as UV photons, charged particles, and excited atoms and molecules. The different control parameters and external setup, including the carrier gas, the discharge electrode configurations, and plasma excitation power sources (alternating current, direct current, or pulse powers), will result in different composition and content of reactive species. Moreover, the composition and abundance of plasma agents vary greatly with the different

types of plasma sources. The overall plasma gas temperature is close to room temperature. As the superior characteristics, the cold plasma has received extensive interest in the agricultural, environmental, and medical applications. The plasma sources used to produce low-temperature plasma are mainly corona discharge, dielectric barrier discharges (DBD), plasma jet, microwave discharge, and gliding arc discharge.

1.2.4.1 Corona Discharge

The corona discharge is local nonequilibrium plasma. The geometric configuration of electrodes plays an important role in corona discharge. The corona discharge generally appears near the tip electrode geometric configuration. The electric field near the electrode is highly nonuniform and large enough to accelerate the randomly generated electrons to the ionization level of the surrounding gas atoms or molecules (Surowsky et al. 2015). The ionization and luminosity are mainly located at the vicinity of the tip electrode, which is called ionization region, or corona layer.

The corona discharge can be driven by the direct current, alternating current, high frequency and pulse power supply. Depending on the number of corona electrodes, there are single electrode corona, double electrodes corona, and multi-electrodes corona. In practical application, the multi-electrodes corona discharge is usually used to increase the production efficiency of reactive species. The steady-state corona discharge consumes very low power (lower than a few Watts) and there is little thermal effect on the treated object surface. Corona discharge has been developed for microbial decontamination, surface treatment, and food processing.

1.2.4.2 Dielectric Barrier Discharge (DBD)

The typical parallel plate dielectric barrier discharge (DBD) device is shown in Fig. 1.2. The parallel plate electrodes are generally covered by one or two dielectric barrier layers, or the dielectric barrier layer is suspended between two electrodes (Fig. 1.2a–c). Figures 1.2d and e show the surface dielectric barrier discharge structure and Fig. 1.2f shows the plate electrode and tip-array electrode covered by one dielectric barrier layer. The DBD usually generates in filamentary mode. When excited by alternating current or pulse power, and the applied electric fields exceed the ignition level, the filamentary discharge is generated randomly between electrodes. Each filament discharge channel can be called a microdischarge. The duration of microdischarges is nanosecond. With the development of microdischarges, the uniform microdischarges distribute in whole air gaps finally.

To describe the overall discharge properties, a simplified equivalent electric circuit is used (Fig. 1.3). When the gap voltage U_g is lower than the ignition voltage (V_D), the discharge will not generate. The equivalent circuit can be regarded as a series connection of two capacitors (the gap capacitance C_g and the capacitance of

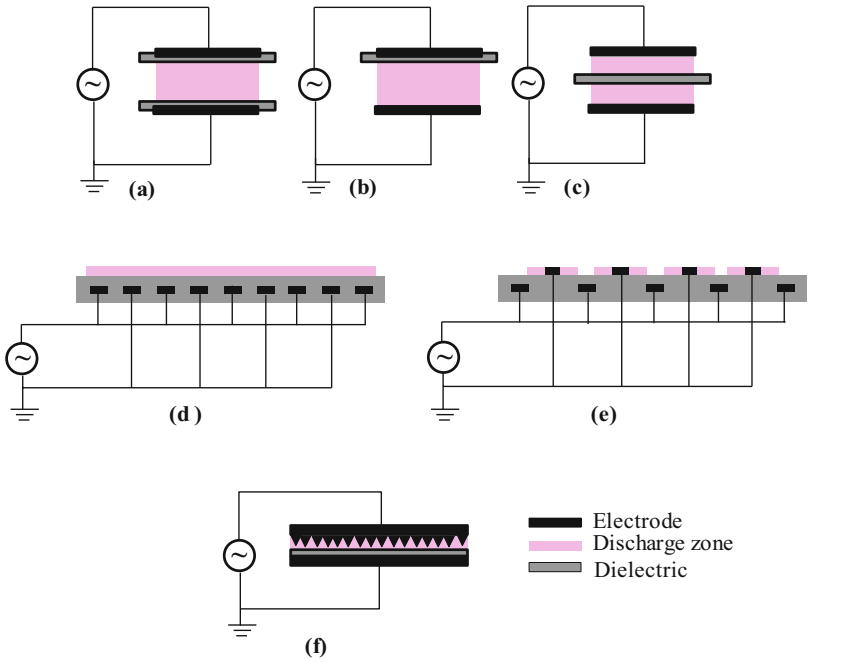

Fig. 1.2 Basic configurations of DBD

Fig. 1.3 Equivalent circuit of DBD load

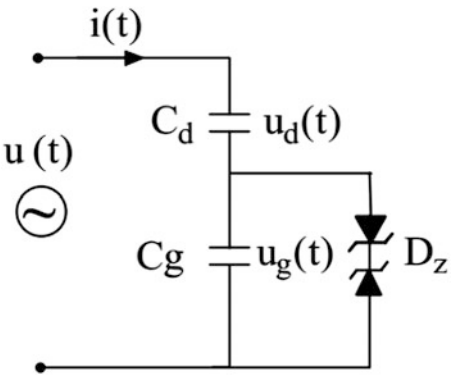

dielectric C_d). The total capacitance C is given by the expression (Wagner et al. 2003).

$$C = \frac{C_d C_g}{C_d + C_g} \tag{1.1}$$

In the microdischarge channel, high-energy electrons will be generated, which will result in the generation of various active species (excited atoms and molecules,

free radicals, and UV photons) and initiate various chemical reactions through a series of processes such as collision, excitation, ionization and so on.

The dielectric barriers can limit the increasing of the conduction current and charge transfer in most applications and thus effectively control the energy of microdischarge. The preferred material of dielectric barrier layer is quartz glass. In special cases, ceramic material and thin enamel layer or polymer layer are also included.

The total DBD current includes the displacement current passing through the dielectric layers and conduction current. The dielectric constant and thickness, and time derivative of the applied voltage (dU/dt), determine the displacement current that can be driven through the dielectric layers. In the ideal case, the displacement current does not consume energy. The conduction current is related to the DBD power.

The average DBD power can be determined by using the voltage charge (V-Q) relation of Lissajous figure. A capacitor (C_M) is connected in series in a DBD peripheral circuit; the voltage at both ends of capacitor is V_M. If the DBD charge delivered by the discharge is Q, the current flowing through the circuit is as follows:

$$I = \frac{dQ}{dt} = \frac{d(C_M V_M)}{dt} = \frac{C_M dV_M}{dt}, \tag{1.2}$$

and the average discharge power can be obtained in Eq. (1.3).

$$P = \frac{1}{T}\int_0^T VIdt = \frac{C_M}{T}\int_0^T V\frac{dV_M}{dt}dt = fC_M \oint VdV_M \tag{1.3}$$

In addition to parallel plate electrode configuration, coaxial dielectric barrier is also commonly used in different applications. The discharge gap typically ranges from 100 μm to several centimeters to meet different environments (Lu et al. 2016b). The applied alternating current (AC) voltage is in the range of hundreds to thousands of volts to initiate the discharge with the frequency up to several MHz between the discharge gaps at atmospheric pressure. Beyond this frequency, the current limitation of the dielectric layers will be less effective and the power consumption will increase rapidly.

Critical Conditions of Dielectric Barrier Discharge

When the load voltage is $u(t) = V_m \sin \omega t$, according to the equivalent circuit analysis, the air gap voltage is as follows:

$$u_g(t) = \frac{C_d}{C_d + C_g} V_m \sin \omega t, \tag{1.4}$$

In a discharge cycle, the discharge will generate when the amplitude of sinusoidal alternating voltage $U_g(t) \geq V_D$ (ignition voltage) is added to the discharge gap.

$$\frac{C_d}{C_d + C_g} V_m \sin \omega t \geq V_D \geq 0, \tag{1.5}$$

$$\sin \omega t \geq \frac{V_D}{V_m}\left(1 + \frac{C_g}{C_d}\right) \geq 0,$$

$$0 \leq \boldsymbol{sin}\ \omega t \leq 1, \quad \text{and} \quad 0 \leq \frac{V_D}{V_m}\left(1 + \frac{C_g}{C_d}\right) \leq 1,$$

The critical conditions of dielectric barrier discharge can be obtained (Eq. 1.6).

$$V_m \geq \frac{(C_d + C_g)V_D}{C_d} \geq 0 \tag{1.6}$$

1.2.4.3 Plasma Jet

The atmospheric pressure nonequilibrium plasma jet (APPJ) generates the plasma through the gas channel and transports the high-energy particles and active species in discharge area to the open space, overcoming the space limitations of traditional plasmas confined between the electrode gap, and creating a direct interaction between plasma jet and object surface with different shapes and sizes. These excellent characteristics make the plasma jet have promising applications in material preparation, plasma medicine, and food preservation industry.

Different plasma jet devices have been developed for the stable generation of nonthermal plasmas for various applications (Reuter et al. 2018; Khlyustova et al. 2019; Yan et al. 2017; Weltmann and Woedtke 2017; Winter et al. 2015). Commonly used DBD configurations (Lu et al. 2012) include coplanar coaxial DBD with two-ring electrodes, single electrode DBD with one-ring electrode, single electrode DBD, and single electrode with one-ring electrode. DBD configurations with electrodes covered by the dielectric layers limit the increasing discharge current through the electrodes and prevent the possible transition to an arc. The plasma jets can extend to the atmospheric environment with the plasma plume length ranging from a few millimeters to more than 10 cm.

As the electric field of coplanar coaxial jet (in Fig. 1.4a) is parallel to the direction of air flow, the plasma jet has the characteristics of lower current and power consumption and long plasma jet length (Nguyen et al. 2019). Figure 1.4b shows the configuration of single electrode DBD with one-ring electrode. The central high voltage (HV) electrode is covered by the dielectric tube with one end closed, and the ring electrode is wrapped outside the dielectric tube. Through this configuration, the electric field intensity in the direction of plasma plume is enhanced, which will

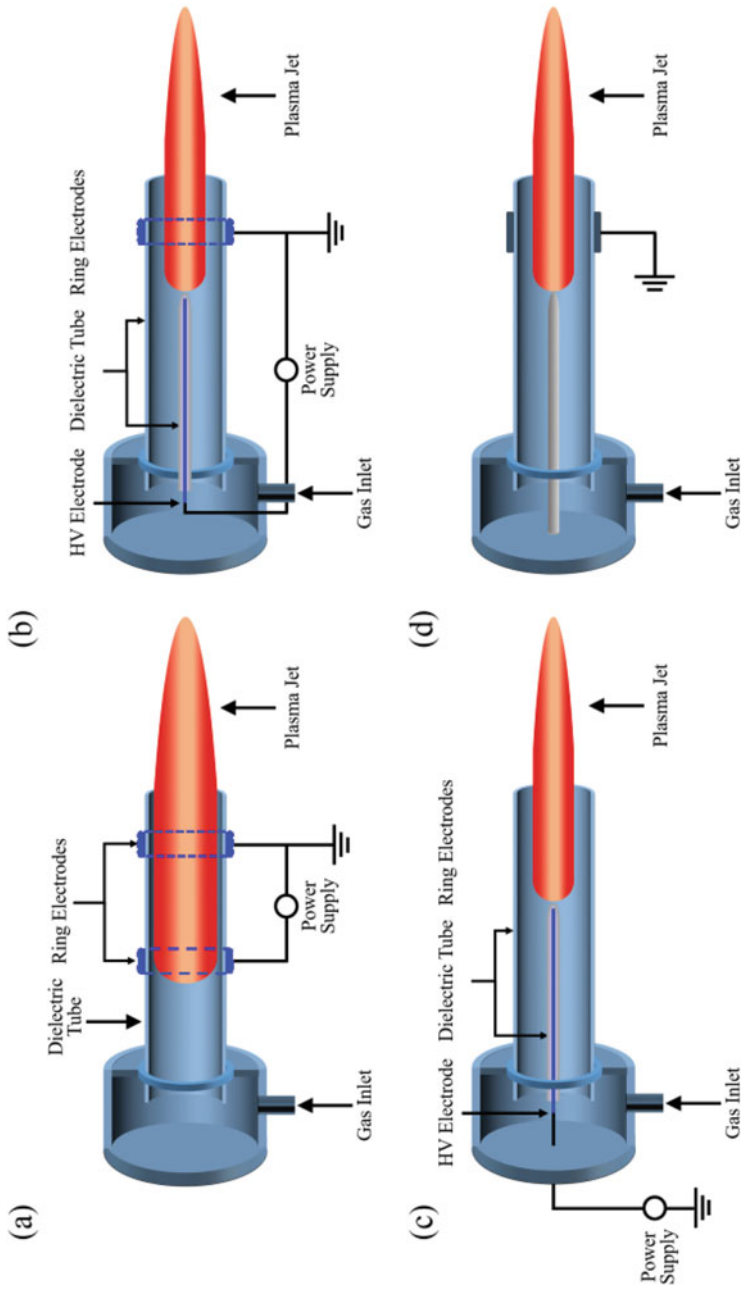

Fig. 1.4 Schematic of a DBD plasma jet. (**a**)The coplanar coaxial jet; (**b**) the single electrode DBD with one-ring electrode jet; (**c**) the single electrode DBD jet; (**d**) the single electrode with one-ring electrode jet

contribute to generate more active species and the plasma jet length. Lu et al. (2008) reported that the helium homogeneous plasma jet was generated with 40 kHz alternating voltage by this electrode configuration, and the length of plasma plume reached up to 11 cm. As shown in Fig. 1.4c, the fact that the electric field of single electrode DBD jet is parallel to the gas flow makes it possible to produce more active plasma chemistry (Walsh and Kong 2008). Fig. 1.4d shows the single electrode with one-ring electrode jet, which is developed for biological and sensitive surface treatment applications (Reuter et al. 2018).

The plasma jets can be generated by applying alternating current (AC), pulsed voltages, and microwaves with the range of frequencies from kHz to radio frequency (RF) and GHz. Generally, noble gases (He and Ar) are used to generate homogeneous plasma jets with low gas temperature. The plasma plume transported into the atmosphere interacts with the nitrogen and oxygen in air. A small amount of nitrogen or oxygen can also be mixed into the noble gases to enhance the production of reactive species (ROS and RNS). Thus, better treatment effects can be obtained in different applications.

High speed intensified charge-coupled device (ICCD) camera with nanosecond exposure time is used to clarify the dynamic propagation process of the discharge and the plume. The snapshots show that the behavior of the plasma plume is not a spatially continuous jet. The propagation of plasma plume appears like discrete plasma bullets traveling at a speed up to 10^5 m/s, which is much higher than the gas flow velocity. The dynamic propagation process of plasma bullets is closely related to the model of the high-density seed electrons and photoionization processes. Research results show that the strong electric field at the head of the bullets plays a vital role in the propagation of bullets. As a result, the plasma bullets are fast propagation ionization waves guided within the discharge channel with the gas flow. The guided ionization waves have the characteristics of repeatability and high reproducibility and propagate along the plasma jet channel (Lu et al. 2016a, b).

As the plume size of the plasma jet is only several millimeters or less, the area treated by the plasma jet is limited to the local surface. To overcome the limited processing area of single plasma jet, the jet array reactor has been developed by assembling multiple jet units. The configurations of jet array reactor include one-dimensional (1D) array with multiple single jets paralleled in line and two-dimensional (2D) honeycomb-shaped arrays (Park et al. 2012). An APPJ array requires careful design and assembly of multiple single jets to meet the needs of treating larger surface at the same time.

1.2.4.4 Microwave Discharge

Compared to the electrode-based plasmas, such as DBD, plasma jet, and corona discharges, microwave-driven discharges can be generated with electrodeless configuration (Surowsky et al. 2015; Ehlbeck et al. 2011). The commercial magnetron (typically operating at a frequency of 2.45 GHz) outputs the microwaves to the process chamber transported by a wave guide or a coaxial cable. The wave guide is

directly coupled to specific discharge device by a resonance cavity. These devices are carefully designed to form the high electrical field in the center of resonance cavity or at the tip of the gas discharge nozzle. The microwave plasma source has the property of the electrons in reaction channel absorbing the microwaves. As a result, the kinetic energy of electrons increases enough to ionize the gas molecular and heavy particles by inelastic collisions. Therefore, the microwave discharge device has the advantage in effective production of high degree ionization and gas molecular dissociation. The electron temperature in the formed plasma core region is about 2×10^4 K and the electron density reaches up to 3×10^{21} m^{-3} (Jasinski et al. 2002). According to the power consumption of microwave plasma, the overall gas temperature ranges from room temperature to several thousand Kelvin. The ignition technique of pulse modulation has been applied to the microwave plasma sources. The pulse modulated atmospheric pressure microwave plasma can keep its original advantages and control the overall gas temperature by adjusting the pulse duty cycle.

The microwave plasma can be excited in the atmospheric environment with noble gases, the admixtures of noble gas and nitrogen, oxygen, and air, or even water vapor. The gas flow rate is in a moderate range of standard liter per minute (slm). According to the gas composition of discharge, the rich reactive species can be induced (such as OH radicals, O_3, O_2^-, and N_xO_y) (Uhm et al. 2006). Similar to plasma jet, microwave plasma has the limitation of small processing space. For large area surface treatment and decontamination, microwave plasma array can be used to solve this limitation (Ekezie et al. 2017).

1.2.4.5 Gliding Arc Discharge

The typical gliding arc reactor is composed of two knife-shaped electrodes. The gliding arc is initiated at the upstream narrowest gap corresponding to the position of the highest electric field, and then the arc slides downstream of the electrodes by the force of gas flow. Depending on the different parameters, gliding arc discharge (GAD) can generate the thermal or nonthermal plasma. In practical application, the gliding arc is generally in the transitional nonequilibrium state with high electron density (above 10^{15} cm^{-3}, Zhu et al. 2018; Roy et al. 2018). It is found that the electric field and air flow affect the moving characteristics of the gliding arc. The results show that the gliding velocity increases with the increase of gas flow velocity, and the gliding arc propagation distance increases and the arc discharge channel becomes more concentrated with the increase of electric field pulse repetition frequency.

However, in the 2D knife electrode reactor, the contact area between the gliding arc and the medium gas is small, and the residence time of gas in the reactor is relatively short, resulting in the low conversion rate of reaction gas, which limits the industrial application of 2D knife gliding arc plasma. In order to improve the planar structure of the 2D knife electrode, a multi-electrode gliding arc reactor (such as three electrodes or six electrodes) has been developed to increase the volume of reaction arc region. In the gliding arc, the swirling flow (the forward vortex flow or

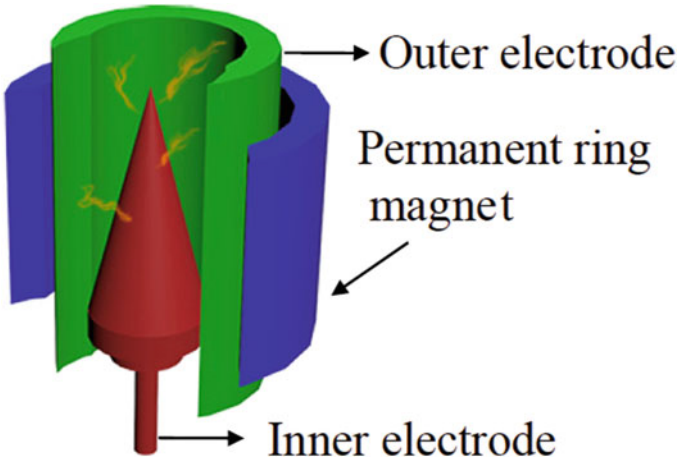

Fig. 1.5 The schematic of rotating gliding arc reactor

the reverse vortex flow) can be formed by tangential gas inlet, which increases the residence time of gas in the GAD reactor. At the same time, the reactive species produced by the gliding arc are uniformly distributed in the circumferential direction, which can make all the medium gases fully interact with the plasma, so as to improve the reaction efficiency. In addition, a magnetically stabilized gliding arc reactor coupled with reverse gas flow is designed to generate stable plasma arc in nonequilibrium regime (Wu et al. 2015). A novel rotating gliding arc reactor coupled by an external ring magnetic field and the tangential gas flow has been developed to further enlarge and stabilize the plasma discharge region (Fig. 1.5).

1.3 Diagnostics and Numerical Simulations of Cold Plasma

Atmospheric pressure cold plasma most often generates in different carrier gas including helium, argon, air, oxygen, nitrogen, or their admixtures in ambient air. The electrons are accelerated in an electric field, and the kinetic energy of electrons increases enough to excite/ionize ground-state atoms and ionize the gas molecules by inelastic collisions which result in the generation of reactive species. The cold plasma is widely used in plasma agriculture, food preservation, material preparation, and plasma medicine. In practical industrial applications, different plasma sources, discharge modes, powers, gas compositions, and plasma interaction modes will affect the physicochemical characteristics of plasma, such as electron density, electron energy distribution, electron temperature, and thus the composition and content of reactive species in gas phase and their final biological effects.

In recent years, different diagnostic methods are employed to characterize plasma dynamic properties (such as the plasma generation and transport process, initiating the production of reactive species and complex chemistry) with the aim of better

understanding and controlling plasmas. The spatially and temporally resolved diagnostics of electric field intensity, electron density, reactive species densities, and related physical and chemical mechanisms have been studied. Diagnostics are very important to the development and optimization of new plasma applications. The diagnostic results may contribute to the development of new plasma model, be the valid input to model calculations, or validation of the correctness of the simulation. The different diagnostics include optical emission spectroscopy, laser-induced fluorescence, mass spectrometry, optical absorption spectroscopy, and electron paramagnetic resonance spectroscopy (EPR). The optical emission spectroscopy, laser-induced fluorescence, and optical absorption spectroscopy are optics-based diagnostic techniques.

1.3.1 Diagnostics in Gas Phase

1.3.1.1 Optical Emission Spectroscopy (OES)

Optical emission spectroscopy is a noninvasive diagnostic technique. It is the most commonly used diagnostic method with easy-to-setup features. Emission spectroscopy of plasma discharge can only probe the excited species as it detects the photons emitted by electronic transitions of atoms or molecules in the excited state in the plasma. The emission spectrum includes much valuable information of the radiating species: firstly, the wavelength of emission spectrum, from which the excited species in the plasma can be determined; secondly, the absolute and relative line intensities and the intensity distribution of the spectral line can be analyzed; thirdly, the spectral line profile of plasma is closely related to the different broadening mechanisms. Thus, emission spectroscopy is an ideal method to diagnose various plasma physical properties, such as excitation temperature, electron density, plasma gas temperature, rotation and vibration temperatures, and even dynamic plasma processes with external synchronous signal unit.

The excitation temperature is an important parameter for the description of the population of electron energy levels in plasma discharge, which is directly related to the plasma physical and chemical process.

When the plasma satisfies the local thermal equilibrium (LTE model), the particle distribution of each energy level (m and n level) obeys Boltzmann distribution law.

$$\frac{N_m}{N_n} = \frac{g_m}{g_n} \exp\left(-\frac{E_m - E_n}{kT_{\text{exc}}}\right) \tag{1.7}$$

With the electron transitions from energy level $m \rightarrow n$, the radiation intensity can be expressed as:

$$I_{\mathrm{mn}} = N_m hc\nu_{mn} A_{mn} \tag{1.8}$$

$$\begin{aligned} I_{mn} &= N_n \frac{N_m}{N_n} hc\nu_{mn} A_{mn} \\ &= N_{\mathrm{n}} \frac{g_m}{g_n} \exp\left(-\frac{E_m - E_n}{kT_{\mathrm{exc}}}\right) hc\nu_{mn} A_{mn} \\ &= N_{\mathrm{n}} \frac{g_m}{g_n \lambda_{\mathrm{mn}}} \exp\left(-\frac{E_m - E_n}{kT_{\mathrm{exc}}}\right) hcA_{mn} \end{aligned} \tag{1.9}$$

$N_{m,}$ $N_{n,}$: the total number of particles at m and n energy level,
g_m, g_n: the statistical weight of the energy level m and n,
A_{mn}: the transition probability,
E_m, E_n: the excitation energy at the m and n energy level,
k: the Boltzmann constant,
ν_{mn}: the wave number of the emission line (energy level $m \rightarrow n$).
Equation (1.10) can be obtained by taking logarithm on both sides:

$$\begin{aligned} \ln \frac{I_{\mathrm{mn}} \lambda_{mn}}{g_m A_{mn}} &= \ln \frac{N_n hc}{g_n} - \frac{E}{kT_{\mathrm{exc}}} \\ &= -\frac{E}{kT_{\mathrm{exc}}} + C \end{aligned} \tag{1.10}$$

The excitation temperature can be approximated to the electron temperature, which means that the cold plasma can induce a series of physical and chemical reactions to meet different application requirements.

The electron density (n_e) can be obtained by the Stark broadening of the H_β emission line at 486.1 nm. The detected H_β profile line is closely related to various broadening mechanisms including natural, instrumental ($\Delta\lambda_I$), Doppler ($\Delta\lambda_D$), Stark ($\Delta\lambda_S$), and Van der Waals ($\Delta\lambda_V$) broadenings. The H_β profiles line is determined by Gaussian (Doppler and instrumental) and Lorentzian (Stark, Van der Waals, and Natural) broadening mechanisms, and their contribution to the profile line broadening can be fitted to the Voigt profile.

The full-width at half-maximum (FWHM) of Gauss, Lorentz, and Vogt profiles has the following properties (Torres et al. 2007; Jovicevic et al. 2000):

1. The convolution of two Gaussian profiles is also a Gaussian profile

$$\Delta\lambda_G^2 = \Delta\lambda_{G1}^2 + \Delta\lambda_{G2}^2 \tag{1.11}$$

2. The convolution of two Lorentz profile, its FWHM is the sum of each Lorentz line

$$\Delta\lambda_L = \Delta\lambda_S + \Delta\lambda_V \tag{1.12}$$

3. The FWHM of Voigt profile can be expressed as follows:

$$\Delta\lambda_{\text{Voigt}} \approx \left[\left(\frac{\Delta\lambda_L}{2}\right)^2 + \Delta\lambda_G^2\right]^{\frac{1}{2}} + \frac{\Delta\lambda_L}{2} \tag{1.13}$$

Therefore, the electron density can be determined by the FWHM of Stark broadening (Zhu et al. 2008).

$$\Delta\lambda_S(\text{nm}) = 2 \times 10^{-11}(n_e)^{2/3}, \tag{1.14}$$

When cold plasma is generated in ambient air, the gas temperature in the discharge zone and the afterglow zone is an important parameter in industrial application. An emission line is characterized by the wavelength, intensity, lineshape, and width. The spectra of OH radicals ($A^2\sum - X^2\prod 0,0$) and N_2 second positive system ($C^3\prod_u - B^3\sum_g$) are a generally used technique to determine the plasma rotational and vibrational temperatures by the best fit between experimental and simulated emission spectra. The gas temperature is approximately the rotational temperature, as the lifetime of these species is much longer than the rotational-to-translational energy transfer typical time in ambient air (Zhu et al. 2008). Generally, the rotational temperature is at room temperature, while the vibrational temperature is much higher than the rotational temperature (about 2000 K) which means that the plasma is in nonequilibrium state and is conducive to enhance the plasma chemical reactions.

The optical imaging diagnostics can characterize plasma morphology and its spatially and temporally resolved development with noninvasive technique. The ICCD camera is a commonly used method for dynamic characteristics of plasma discharge. With the ICCD photos, in-line characteristics of plasma sources, such as the morphology and development of streamers and branching, the transitions of glow discharge to arc, and the spatial structure of the DBD microdischarge channel, can be studied in detail. As the typical time-modulated power supply excitation of plasma, phase-resolved OES (PROES) methods are needed to synchronize the plasma discharge and the ICCD camera (Reuter et al. 2018; Bruggeman and Brandenburg 2013).

The AC power supply is synchronized with TTL signal generator (to obtain temporal resolution), while the ICCD camera is controlled by the digital delay signal (as the gating signal of ICCD camera to obtain spatial resolution). By changing the delay time with respect to the TTL synchronous signal phase resolution is obtained. Generally, the ICCD camera is equipped with different band pass filters to capture

images of specific active species in excited state with different time resolution. Combined PROES and electrical characterization can give clues to the main plasma characteristics, the dynamic processes of discharge development, and spatial-temporal behavior of excited reactive species in plasma.

With this technology, the ICCD diagnostic results show that the development of plasma jet is just like the discrete plasma bullets. The dynamic excitation processes and different discharge modes of the RF-driven plasma jet with He and Ar carrier gases have been investigated (Lu et al. 2016a, b; Benedikt et al. 2010). The predominant production mechanisms and spatial-temporal distribution of the excited radicals in the plasma discharge have been reported elsewhere (Barletta et al. 2020). It is obvious that some radicals have almost the same distribution in streamer shape, emission space distribution, and relative intensity. The possible generation mechanisms of the excited state radicals are described in detail.

1.3.1.2 Laser-Induced Fluorescence

The cold plasmas excited in ambient air are widely used in the fields of material surface modification, biological treatments, postharvest preservations, and water purification. By changing different gas compositions (such as air, oxygen, nitrogen, helium, argon, or their admixtures), the desired reactive species (ROS/RNS) will be produced to meet different application requirements and improve processing efficiency. It has been reported that radicals (e.g., OH, O, and NO) are key reactive agents associated with biomolecule modification, bactericidal effects, and organic degradation for their high oxidation and biological effect. Thus it is important to investigate the density distribution and temporal behaviors of reactive species (e.g., OH, O, and NO).

As mentioned previously, optical emission spectroscopy can detect the spectrally resolved emission lines of excited species. However, most of the reactive species in plasma may be in the ground states. Laser-induced fluorescence (LIF) is a perfect technique for characterizing the absolute density and its temporal-and-spatial dynamics of the reactive species in the ground states. Quantitative researches of species in the ground state are conducive to better evaluation of the roles of the reactive species during plasma treatment.

Laser-induced fluorescence emits fluorescence signal from atoms or molecules excited by laser photon. If the molecules or atoms in the electronic initial state absorb one laser photon with energy hv, they will be excited to the upper electronic state. The upper unstable state will decay spontaneously to a lower state by radiating another photon with energy hv. The fluorescence spectral radiant power, $\Phi_F(v)$ (Daily 1997), is.

$$\Phi_F(\nu) = \varepsilon h\nu\left(\frac{A_{21}}{4\pi}\right)\Omega_C \int_{V_C} N_2\varphi(\nu)dV_C \tag{1.15}$$

where ε is the efficiency of the collection optics, h Planck's constant, v the optical transition frequency, A_{21} the Einstein coefficient, Ω_c the solid angle of the collection optics, N_2 the population of the excited state by laser excitation, and φ(v) the normalized line shape function describing the spectral distribution of the emitted fluorescence.

The total fluorescence radiant energy (Q_F) collected by the detector will be

$$Q_F = \int_{\Delta t}\int_{\Delta v_{\mathrm{Det}}} \Phi_{\mathrm{F}}(v)\, dvdt \tag{1.16}$$

The total fluorescence radiant energy (Q_F) can be further expressed as:

$$Q_F = hv\left(\frac{\mathrm{A}_{21}}{4\pi}\right)\Omega_c \int_{V_c}\int_{\Delta v_{\mathrm{Det}}} \varepsilon\varphi(v)dv \int_{\Delta t} N_2(t)dtdV_c \tag{1.17}$$

We can define a calibration constant

$$C = hv\left(\frac{A_{21}}{4\pi}\right)\Omega_c \int_{V_c}\int_{\Delta v_{\mathrm{Det}}} \varepsilon\varphi(v)dvdV_c \tag{1.18}$$

then

$$Q_F = C\int_{\Delta t}\int_{V_c} N_2(t)dV_c dt \tag{1.19}$$

The fluorescence process may occur in two-level or multi-level atoms and molecules. If different transitions of two-level or multi-level atoms and molecules are excited in sequence and the corresponding fluorescence signals can be observed, the fluorescence spectrum of the reactive species in the ground states can be obtained. Thus, the total fluorescence radiant energy collected from each transition can be calculated by Eq. (1.19).

The absolute concentrations of the species in the ground states can be obtained by calibrating the known content of species with similar energy levels and excitation coefficients or by the decay model of LIF signals (Laroussi et al. 2017). For example, the absolute atomic oxygen density can be obtained by introducing a known xenon density in the plasma reactor (Sousa and Puech 2013).

The absolute density of OH, O, and NO in plasma with different discharge devices, gas composition, and excitation power supply has been successfully studied using laser-induced fluorescence technology (Li et al. 2016; Jiang and Carter 2014; Gessel et al. 2013).

1.3.1.3 Mass Spectrometer

A mass spectrometer (MS) is composed of sampling system, the vacuum system, the ion source, the mass analyzer, the detector, and the computer sampling and control system (in Fig. 1.6). MS can measure the positive ions, negative ions, and neutral species generated in plasma, and their kinetic energy and evolution in microsecond time scales, which is beneficial to study different species and their subsequent chemistry. The use of MS to detect ions and radicals is well demonstrated in low-pressure plasma (Benedikt 2010); however, its application to atmospheric pressure cold plasmas is still a challenge. As the central part of the mass spectrometer needs low pressure, the instrument used for detecting atmospheric cold plasma requires the gradient decompression interface. The neutral particles and energetic ions produced in atmospheric cold plasma are sampled using a three-stage differentially pumped molecular beam inlet system with skimmer cones and turbo molecular pumps. The three pressure decompression stages (P_1, P_2, and P_3 stages) provide a decompression process from atmospheric pressure to 0.9 Torr at the P_1, 6×10^{-5} Torr at the P_2, and the 3.1×10^{-7} Torr at the P_3 stage (in Fig. 1.7. Jun-Seok et al. 2011; Jiang et al. 2020).

A mechanical beam chopper is positioned between the second and third pumping stages. When the beam chopper is closed, the residual gas is measured in the mass spectrometer which is regarded as the background signals. The background signals are subtracted from the measurements with the beam chopper in open state (Stoffels et al. 2007).

The analysis of sampled ions and neutrals operates in different mode. The neutral particles are measured in the residual gas analyzer (RGA) mode, while the ions are detected in the secondary ion mass spectrometer (SIMS) mode.

In the case of neutral particles in plasma, all ions sampled in the mass spectrometer are excluded by applying appropriate external bias voltages to the extractor and other electrodes mounted between the sample orifice and the internal ion source. The instrument is equipped with an internal ionization source with the variable electron energy, and the sampled neutral species are then ionized to generate charged particles. The ionization mechanisms include the generation of positive ions by

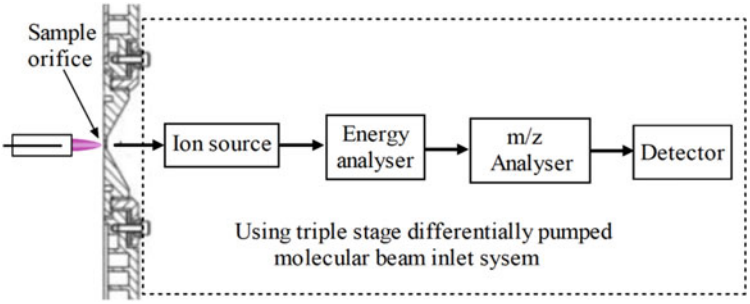

Fig. 1.6 The process of mass spectrometer for plasma analysis

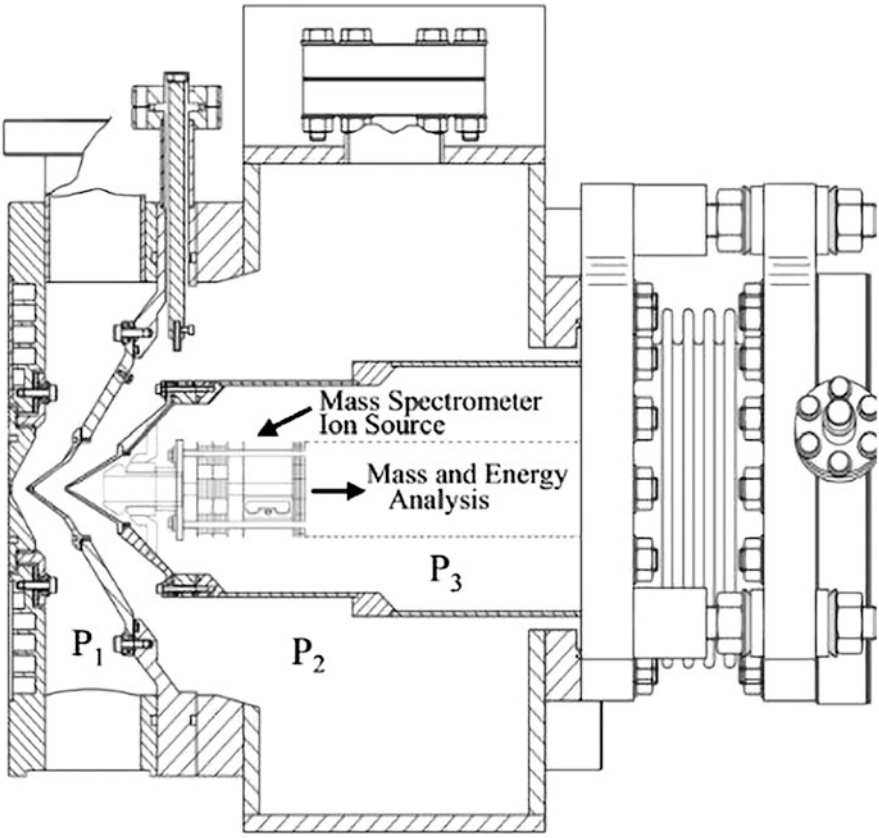

Fig. 1.7 Schematic of mass spectrometer analyzer

electron impact ionization and negative ions by electron attachment or ion-pair production. In the case of ions measurement mode, the ionization source of mass spectrometer is turned off and only ions generated in the plasma are detected in the internal (Rees et al. 2010; Stoffels et al. 2007).

All ions are then transmitted through the energy analyzer (generally optional for the detection of neutrals) and *m/z* analyzer and finally reach the detector. As a result, the detected electrical signals of the current or TTL pulses are obtained. Combined with the ion energy analyzer, the energy distribution information of various ions in the system can also be given.

The electron energy of mass spectrometry ionization source can be controlled by "soft ionization" and "threshold ionization" techniques. As to the soft ionization, the energy can be set separately from the ionization appearance potential to tens of eV. It is effective to preferentially ionize traces of low ionization potentials. There will be much higher concentration of low ionization energy compared with that of larger ionization potentials if the applied energy decreases gradually. As to the threshold

ionization, the electron energies range from just below the threshold of ionization potentials to 10 or 20 eV (Rees et al. 2010). It is useful for a detailed investigation of the generation of active species and subsequent chemistry.

1.3.1.4 Fourier Transform Infrared Spectroscopy

Fourier transform infrared (FTIR) spectroscopy is a useful technology to probe the chemical structure of molecules by identifying the vibrational frequencies of chemical functional groups in the gas, liquid, and solid phases. An interest has grown in recent years to characterize gaseous chemical composition variation in cold plasma using FTIR spectroscopy. FTIR spectroscopy provides quantitative analysis of the concentration of gaseous species based on the Beer-Lambert law, which can establish the correlations between species generated in plasma and their infrared absorption spectrum. This technique has the advantage of detecting different intermediate species generated in the progress of chemical reactions.

In the mid-infrared region, two main vibrations of chemical groups include the stretching vibrations and the bending vibrations. The stretching vibrations vibrate along the chemical bonds, which are related with bond length changes. The bending vibrations are relevant to bond angle changes (δ in plane, π out of plane).

The harmonic oscillator model can be used to describe the stretching vibrations. The chemical bonds are expressed by two point masses connected by a spring. The bond strength is the spring tension k and the point masses (m_1 and m_2) model represent the masses of the chemical groups related with bonds. The oscillation frequency v is as follows:

$$v = \frac{1}{2\pi c}\sqrt{k\frac{(m_1 + m_2)}{m_1 m_2}} \tag{1.20}$$

where c is the speed of light, and k is the bond strength (Berthomieu and Hienerwadel 2009).

Thus, the oscillation frequency greatly depends on the type of chemical groups and the type of chemical bonds. Therefore, the clear relationship between infrared vibrational frequencies and the structural properties of a given chemical groups is established. It is very convenient to characterize gas chemical composition variation in plasma discharge using FTIR spectroscopy.

1.3.2 Diagnostics in Liquid Phase

1.3.2.1 Electron Spin Resonance Spectroscopy

Electron spin resonance (ESR) spectroscopy or electron paramagnetic resonance (EPR) spectroscopy is the specific technology for detecting samples with at least one unpaired electron. The ESR spectroscopy is effective to study the structure of solid and liquid substance. It is widely used to characterize the formation of free radicals and the possible dynamic chemical processes induced by cold plasma in liquid phase recent years.

When the electron spin is in the external magnetic field B, the interaction energy E exists between the spin magnetic moment (μ_s) and the external magnetic field is:

$$E = -\mu_s \cdot B = g_e \mu_B S \cdot B/\hbar \tag{1.21}$$

If the direction of the magnetic field B is chosen as the Z axis of the coordinate system and the magnetic field strength is B_0, the energy expression is as follows:

$$E = g_e \mu_B S_Z B_0/\hbar = m_s g_e \mu_B B_0 \tag{22}$$

where g_e is the electron g factor (2.0023 for a free electron), μ_B is the Bohr magnetron (9.274 × 10–28 J G^{-1}), and ħ is the Planck constant. The g factor contains important information about the electron spin. S_Z is the component of spin on the Z axis, $S_Z = m_s\hbar$. The electron spin quantum number m_s takes the values $m_s = 1/2$, and $m_s = -1/2$, which correspond to two energy levels, and the corresponding energies are $E_2 = 1/2 g_e \mu_B B_0$, $E_1 = -1/2 g_e \mu_B B_0$ respectively. The difference in energy ($\triangle E$) between the two electron spin levels is:

$$\Delta E = E_2 - E_1 = g_e \mu_B B_0 \tag{1.23}$$

The unpaired electrons will absorb the microwave electromagnetic wave energy (the frequency is ν). If the microwave frequency ν can meet the expression $\hbar\nu = \Delta E = E_2 - E_1 = g_e \mu_B B_0$, the electrons at the low-energy level will jump to the high-energy level, and the spin resonance occurs. One transition of electrons produces a resonant absorption signal. Generally, the microwave frequency ν is fixed as a constant in the test, and the magnetic field intensity is scanned until the resonant conditions are matched (Wang et al. 2011).

In general, free radicals are unstable and the lifetime of radicals is very short. Thus, it is difficult to be detected, especially in liquid. The spin trapping technique is used, which involves the addition of a spin trapping agent reacting with free radicals to form relatively stable spin adducts. Then the spin adducts can be detected by ESR spectrometer.

1.3.2.2 Spectrophotometry

Spectrophotometry is a method for the qualitative and quantitative analysis of a substance by determining its absorbance or luminous intensity at a specific wavelength or within a certain wavelength range. The testing principle is based on the Beer-Lambert law. Some reactive species have characteristic wavelengths with high absorption coefficient in common wavebands. For example, the absorption coefficient of HO_2 at 230 nm ultraviolet light is as high as 1400 M^{-1} cm^{-1} (Bieiski et al. 1985). However, reactive species in the liquid have a relatively low concentration and a short half-life. Additionally, different reactive species may absorb light of the same wavelength, resulting in interference. It is often difficult to detect directly the characteristic wavelength of reactive species in liquid. In general, most spectrophotometric measurements use chromogenic agents, that is, new long-lived species are produced by the reaction of specific chromogenic agents with reactive species to be measured, so as to improve the detection sensitivity and avoid mutual interference. Lukes et al. (2014) used titanium sulfate as the chromogenic agent and obtained the concentration of H_2O_2 by measuring the absorbance at 407 nm. This chromogenic agent is only effective for H_2O_2, so it will not be interfered by other compounds in the liquid. It is reported that the long-lived active species measured by spectrophotometry mainly include H_2O_2, O_3, nitrate, and nitrite, and the short-lived active substances include OH, HO_2, etc. (Bieiski et al. 1985; Machala et al. 2013; Von et al. 2012).

1.3.3 Numerical Simulations

Various plasma sources generate cold plasma discharge at atmospheric pressure for both fundamental researches (discharge characteristics, physicochemical reaction mechanisms) and application-focused study (such as plasma agriculture, food preservation, material preparation, and plasma medicine). Different operating parameters (excitation power supply, carrier gas or even mixed with water vapor, discharge power, gas flow rate, and plasma treatment mode) will affect the type and concentration of reactive species (ROS/RNS) in gas phase, and result in different application effects for treating solid surfaces.

In practical applications, plasmas need to be generated in humid, gas-liquid or even liquid phase environments, as the surface of the object to be treated is covered with liquid or even immersed in aqueous solution. A lot of water vapor will inevitably mix into the carrier gas above the liquid in this case. The plasma-liquid generation system may include gas phase plasma with different carrier gases and mixed water vapor, plasma-liquid interaction interface (plasmas generate over the liquid surface or in the continuous carrier gas channel contacted with the liquid), and the liquid phase region. The plasma discharge will produce various reactive species (ROS/RNS) and initiate a series of physical and chemical reactions in the gas phase

and at gas-liquid interface. The reaction products in gas phase can be directly diffused into the liquid phase or transported into liquid phase by various transfer processes (Bruggeman et al. 2016; Zhou et al. 2018).

The rich reactive species (ROS/RNS) generated in gas plasma, physicochemical processes coupled with the plasma liquid interaction, aqueous reactive species induced by gas plasmas, and subsequently chemical reactions in liquid phase play an important role in various plasma applications. It is necessary to have a detailed understanding of the kinetic process of plasma discharge with gas-liquid interactions to make more effective use of the advantages of atmospheric cold plasma applications.

As mentioned above, many diagnostic techniques are used to characterize plasma dynamic properties, the complex reactions, and the formation of reactive species in the gas phase and liquid phase region. Though many studies have been carried out, the production mechanism and the temporal and spatial distribution of reactive species in gas phase and liquid phase are still not well understood. Plasma modeling and simulations, combined with diagnostic techniques and experiments, make great contributions to gain a deeper understanding of the basic characteristics of reaction mechanisms and processes. In particular, direct measurement and diagnosis are costly or difficult to carry out sometimes.

Plasma modeling and simulations may offer useful information including spatial and temporal distribution of radicals and charged particles, reaction rates with various collision processes, mass transfer kinetics, and electric potential and field distribution.

As for simulation, the usually used models are particle model (Teunissen and Ebert 2016; Fierro et al. 2018), fluid model (Koen and Annemie 2017; He and Zhang 2012), and global model (Sun et al. 2019a; Schroter et al. 2018; Murakami et al. 2013). The particle model has the good accuracy; however, the particle model has a larger amount of calculation, takes a longer time, and takes up more resources. Currently, this method is applicable to atmospheric pressure plasma simulation with very small structure in μm scale (Kim et al. 2006) and very short propagation lengths (Stephens et al. 2018). The fluid model is the widely used model at present, which can reflect the internal properties of plasma, but it is also limited by the amount of calculation and algorithm stability. It is mainly used to study the plasma with relatively simple chemical process. The global model greatly reduces the amount of calculation by setting the spatial distribution of active particles, and can simulate and analyze the plasma with complex chemical processes (Lee and Lieberman 1995).

Many researchers have used particle, fluid, and global models to study the generation, evolution, and characteristics of plasma, the content and distribution of reactive species with different gas components (or with different water vapor content) in gas phase plasma, as well as the physical and chemical reaction process of gas-liquid plasma and the concentration and distribution of reactive species in gas-liquid and liquid phase.

Based on the results of particle simulations, high-energy electrons with about 50 eV electron energy will appear in pulsed microwave frequency plasmas

discharge, which means that this type of discharge has great potential application value. For example, these high-energy electrons may break some chemical bonds, which will bring great convenience to the application of plasma biological sterilization and food preservation. Kwon et al. (2014) report that high-energy electrons with energies larger than 50 eV at the electrode can be generated in pulsed microwave atmospheric microplasmas. The experimental results show that electrons with energy larger than 50 eV may result in DNA double strand breaks in bactericidal process. Lee et al. (2018) show that energetic electrons with energy larger than 10 eV are generated in pulsed microwave helium plasmas, which can break bonds of nitrogen molecules, and helps to form various reactive species efficiently. Wang et al. (2020) have obtained similar results, and the simulations show that high-energy electrons with electron energy greater than 20 eV may be formed in the pulse microwave plasma.

Streamer discharges with needle-to-plane configurations are widely used in various plasma applications. The generation, evolution, and development of streamer discharge are the basic and important physical processes in plasma discharge. Three-dimensional particle model and fluid model have been effectively used to simulate and probe elementary properties of streamer discharges (Sato et al. 2020; Marskar 2020; Teunissen and Ebert 2016; Fierro et al. 2018). Sato et al. (2020) adopted fluid models to study the streamer propagation properties including propagation speed, head size of streamer, and plasma formation with different parameters. Marskar (2020) demonstrates the dynamic morphology properties of positive streamer fluctuations, branching, and the generation of tree-like discharge by the fluid model. Teunissen and Ebert (2016) present dependence of different pulsed discharges morphology on the oxygen content (with different ratio of oxygen to nitrogen) and applied voltage using the particle model. Fierro et al. (2018) show the influence of photoionization on the streamer generation and propagation in nitrogen and helium mixture gas by particle modeling.

The cold plasma most often generates different carrier gases including noble gas, air, oxygen, nitrogen, or their admixtures in ambient air. The presence of oxygen-based and nitrogen-based gases (air, oxygen, nitrogen) are pivotal for the generation of reactive oxygen species and reactive nitrogen species (RONS), and these reactive species are effective for different applications. In addition, due to the influence of ambient humidity, water vapor will inevitably mix into the plasma generation system. When the plasma interacts with the aqueous solution, much water vapor will be produced and mixed into the carrier gas. The introduction of water vapor will affect the plasma dynamics, or as a precursor for inducing complex chemical reactions tends to produce rich reactive oxygen-based and nitrogen-based species. The plasma dynamics, the fundamental chemical reaction process, and final generation of reactive species in gas phase have been widely researched experimentally and numerically for better application efficiency.

Previous numerical simulations based on the fluid model have been adopted to characterize dynamic plasma chemistry in He with different gas admixture, such as air, oxygen, and water vapor (Liu et al. 2020; Yang et al. 2014; Waskoenig et al. 2010; He and Zhang 2012; Lietz and Kushner 2018). Global models effectively

simulate bulk plasma properties and complex plasma chemical reactions by carefully considering the plasma boundary conditions. Global models have already been successfully improved and applied to investigate the plasma chemistry of Ar with humid air admixture (Gaens and Bogaerts 2014), Ar with water vapor admixture (Tavant and Lieberman 2016), He-O_2 with humid air (Murakami et al. 2013), He-O_2 with water vapor (Liu et al. 2011), He with air admixture (Sun et al. 2019a), He-air with water vapor (Sun et al. 2019b), and He with water vapor (Liu et al. 2010). Numerical simulation of different models provides insights into plasma dynamics, the production rates and densities of reactive species, key reactive species, and their chemical reaction process.

The modeling and simulation of interaction between plasma and liquid may involve gas phase plasma generation, plasma-liquid interface, and the liquid phase region. The mass transfer processes are generally supposed to be carried out through the thin plasma-liquid interaction layer between the gas and liquid phases by different transfer mechanisms (such as diffusion, solvation, absorption, desorption, and their chemical reactions). Many researchers have used different models from zero dimension to multidimensional to simulate the interaction mechanism between plasma and liquid.

Chen et al. (2014) adopt the 1D diffusion-drift fluid model to simulate the plasma-liquid chemistry with highly hydrous biofilm. The results show that the mass transfer of reactive species in the liquid region can penetrate to a depth of 40–50 μm. A similar model is used to show the depth distribution of five main reactive species (OH, O_3, HO_2, O_2^-, and H_2O_2, Jiang et al. 2016) in liquid. Tian and Kushner (2014) use the *nonPDPSIM* (the multi-fluid 2D hydrodynamics model) to study the interaction of plasmas with the thin water layer of 200 μm covering tissue. The simulation results indicate that the important reactive species, such as $ONOO^-$, NO_3^-, O_3, and H_2O_2, may reach the underlying tissue covered by thinner water layer after a few seconds.

The interaction processes between plasma and liquid have recently been researched using global models. Lee et al. (2013) study the chemical reaction mechanisms at the interface between the plasma and distilled water or H_2O_2 by global model. The computational results show that distilled water mixed with hydrogen peroxide increases the formation of hydroxyl radicals. Hamaguchi (2013) reports the liquid phase chemical products initiated by gas plasma. The combined dissolution of OH and NO in liquid will initiate a series of chemical reactions and generates more reactive species (O_2^-, ONOOH, HNO_3, HNO_3, and so on) in liquid than that of only OH or NO.

1.4 Formation of Reactive Species in Liquid

1.4.1 Formation Mechanisms of Main Reactive Species in Liquid

The cold plasma generated in ambient air is the rich reactive species source. When gas plasma interacts with liquid, it will initiate a series of physical and chemical processes and generate various reactive species above or at gas-liquid interface which can dissolve into liquid phase directly or transport into liquid phase by interphase mass transfer processes and finally determine the different productions in liquid phase. Therefore, the liquid products are closely related to the reactive species excited in gas plasma, gas-liquid interaction and reaction process, and gas-liquid mass transfer process.

Reactive oxygen species, such as OH radical, active oxygen atom, hydrogen peroxide, and ozone, are generally considered to play an important role in practical applications of cold plasmas. Reactive nitrogen species including nitrite, nitrate, and peroxynitrite are generated by a series of chain reactions based on NO_x and liquid. The formation of RNS will increase the acidification of plasma-treated liquid, and this may also generate synergistic effects.

The gas composition (such as helium, argon, air, oxygen, nitrogen, or their admixtures in ambient air) is an important consideration that determines the final production of reactive species in plasma-treated liquid.

At the gas-liquid interface, the gas phase plasma interacts with the liquid, and the reactive species can be generated by electron impact excitation and dissociation of water molecules and gas molecules.

The generation of gaseous OH radicals is through dissociation of water molecules with metastable Ar, He, and N_2 (Nikiforov et al. 2011; Shen et al. 2015; Zhang et al. 2017),

$$e + H_2O \rightarrow H + OH + e \tag{1.24}$$

$$Ar^* + H_2O \rightarrow Ar + H + OH, \tag{1.25}$$

$$He * + H_2O \rightarrow He + H + OH, \tag{1.26}$$

$$e + N_2 \rightarrow N_2{}^* + e \tag{1.27}$$

$$N_2{}^* + H_2O \rightarrow N_2 + OH + H \tag{1.28}$$

OH radicals can also be produced by plasma-initiated ionization of water followed by combination with another water molecule and as a result generate H_3O^+ and the OH radical (Shen et al. 2015; Zhang et al. 2017),

$$e + H_2O \rightarrow H_2O^+ + 2e, \tag{1.29}$$

$$Ar^{+} + H_2O \rightarrow H_2O^{+} + Ar, \tag{1.30}$$

$$H_2O^{+} + H_2O \rightarrow H_3O^{+} + OH. \tag{1.31}$$

When oxygen and air is used as carrier gas, OH radicals can be produced by the reaction of active oxygen atoms (dissociation of oxygen) with water molecules (Lukes and Locke 2005).

$$e + O_2 \rightarrow O\left(^3P\right) + O\left(^3P\right) + e \tag{1.32}$$

$$e^{-} + O_2 \rightarrow O\left(^1D\right) + O\left(^3P\right) + e \tag{1.33}$$

$$O\left(^1D\right) + H_2O \rightarrow OH + OH \tag{1.34}$$

It is the complex chemical reaction processes at gas-liquid interface. Thenitrogen-based reactive species will be induced in gas plasma, such as nitric oxide, nitrogen dioxide, and active nitrogen atom, which will result in the quenching of OH radicals by reactions of 1.351.361.37 (Dorai and Kushner 2003; Machala et al. 2013).

$$N + OH \rightarrow NO + H \tag{1.35}$$

$$OH + NO + M \rightarrow HNO_2 + M \tag{1.36}$$

$$OH + NO_2 \rightarrow ONOOH \tag{1.37}$$

The formation of hydrogen peroxide in liquid may originate from the recombination of OH radicals induced by the gas liquid plasma discharge.

$$OH + OH \rightarrow H_2O_2 \tag{1.38}$$

$$O_2 + O + M \rightarrow O_3 + M \tag{1.39}$$

The ozone generation in gas phase involves three body collision processes such as oxygen molecule, the ground-state atomic oxygen, and a collider M. The formation of ozone is probably affected by the relative humidity of the gas-liquid plasma discharge. A lot of water vapor will be produced above or at gas-liquid interface when plasma discharge is excited. Water vapor will reduce the energy of electrons in gas plasma, thus affecting the process of ozone generation. The ozone generated in gas plasma can dissolve into liquid by the gas-liquid mass transfer process.

When air or nitrogen with different oxygen admixture is used as the carrier gas, the oxygen atoms will be quenched by reaction with active nitrogen atoms, nitrogen, and nitric oxide, which are favorable for the formation of ozone and hydroxyl groups (Eqs. (1.44), (1.45), (1.47)). Meanwhile, the formation of active nitrogen atoms and nitric oxide in gas plasma will lead to the destruction of ozone by Eqs. (1.40), (1.41) (Lukes and Locke 2005).

$$N + O_3 \rightarrow NO + O_2 \tag{1.40}$$

$$NO + O_3 \rightarrow NO_2 + O_2 \tag{1.41}$$

Nitrogen oxides can be generated from the gas-liquid plasma discharge by dissociated nitrogen and oxygen (Du et al. 2008).

$$e + N_2 \rightarrow N + N + e \tag{1.42}$$

$$e + O_2 \rightarrow O + O + e \tag{1.43}$$

$$N + O \rightarrow NO \tag{1.44}$$

$$N_2 + O \rightarrow NO + N \tag{1.45}$$

$$N + O_2 \rightarrow NO + O \tag{1.46}$$

$$NO + O \rightarrow NO_2 \tag{1.47}$$

Peroxynitrite is generated by reactions (1.37), (1.48), (1.49) in air or nitrogen gas-liquid discharge. Many studies have shown that peroxynitrite has strong oxidation which can react with biological molecules and result in bacterial inactivation.

$$O_2^- + NO \rightarrow ONOO^- \tag{1.48}$$

$$NO_2^- + H_2O_2 \rightarrow ONOOH + H_2O \tag{1.49}$$

Generation and dissolution of nitrogen oxide produced in the air or nitrogen gas-liquid plasma will result in the generation of NO_2^- and nitrate NO_3^- in liquid.

$$2NO_2 + H_2O \rightarrow NO_2^- + NO_3^- + 2H^+ \tag{1.50}$$

$$NO + NO_2 + H_2O \rightarrow 2NO_2^- + 2H^+ \tag{1.51}$$

1.4.2 Efficient and Selectable Production of Reactive Species in Liquid

Different operating parameters, such as excitation power supply, carrier gas or even mixed with water vapor, discharge power, gas flow rate, and plasma treatment mode, will affect the type and concentration of reactive species (ROS/RNS) in liquid phase.

Kanazawa et al. (2011) use pulse power supply and needle plate discharge structure to form gas-liquid plasma above the liquid surface. The evolution process of OH radicals in gas phase plasma over time is obtained by laser-induced fluorescence technology. Meanwhile, the relationship between OH concentration and discharge time in the liquid phase induced by plasma is determined by chemical

detection method. They believe that OH radicals produced in gas phase plasma will be dissolved in the liquid phase. Gorbanev et al. (2016) present that the content of hydrogen peroxide increases rapidly with increased carrier gas humidity (He or He +0.5%O_2). The result shows that hydrogen peroxide is not generated in liquid by dissociation of water, but instead is produced in gas phase plasma and then diffuses into the liquid phase.

Pavlovich et al. (2013) show that the composition of liquid products varies from ozone mode to nitrogen oxide mode with the increase of discharge power density. The content of ozone in liquid is high and the content of hydrogen peroxide is low at low power densities. When the power density increases, the trend is opposite. Lu et al. (2017) use two different discharge modes (needle plate gas-liquid discharge)—filament discharge and uniform discharge—to compare the types and contents of reactive species in liquid treated by air plasma. The results show that H_2O_2 and NO_3^- are the main products in liquid by filamentous discharge, while NO_2^- and NO_3^- are the dominant products in liquid by uniform discharge. Uchida et al. (2016) study the difference of liquid phase products by two different treatment methods of plasma jet contact/no contact with liquid surface. It is found that the content of H_2O_2 in water is much higher than that of NO_2^- when plasma is directly contacted with liquid surface, while the content of NO_2^- in non-contact type is much higher than that of H_2O_2. Tani et al. (2012) study the formation of free radicals in aqueous solution treated by helium plasma jet using spin trapping technique (ESR). The results showed that when oxygen is added in different positions, OH radicals and O_2^- appeared in the aqueous solution, but the relative content of O_2^- is not the same, indicating that the content of free radicals in liquid can be controlled by different plasma sources. Niquet et al. (2018) present the different chemical composition of plasma-treated water (PTW) by microwave plasma and dielectric barrier plasma. The results show that nitrogen-based chemistry play an important role in PTW by a microwave-driven plasma source, with high content of nitrous acid converting to nitrite and nitrate, while hydrogen peroxide and nitrate are main components in PTW by a dielectric barrier discharge system. Dai et al. (2016) develop a point-to-plate discharge device to produce reactive species in liquid efficiently and selectively with Ar and air as the carrier gas. The hydrogen peroxide is the predominant component in Ar plasma, while NO_3^- and NO_2^- are main species generated in air plasma-treated liquid.

As reported by Shen et al. (2019), selective and high-efficacy formation of reactive species is obtained by using air and oxygen as the carrier gas. When plasma is generated in oxygen, only ROS such as OH, O_3, and H_2O_2 are produced. In the air plasma, both RNS (such as NO, NO_2^-, NO_3^-, $ONOO^-$) and ROS are induced in liquid. The content of OH radical in the liquid phase treated by oxygen plasma discharge is much larger than that treated by the air plasma discharge.

As mentioned above, the chemical composition of the liquid products initiated by plasma is affected by the plasma operating parameters. In other words, liquid products can be produced selectively and efficiently by changing corresponding parameters, which play an important role in improving the efficiency of practical applications.

1.5 Conclusions

The cold plasma is widely used in plasma agriculture, food preservation, material preparation, and plasma medicine. In practical applications, it is necessary to have a deep understanding of plasma generation, characteristics, gas-liquid interaction, mass transfer process, and the final liquid products in order to obtain desired effects. Plasma modeling and simulations, combined with diagnostic techniques, are helpful to understand plasma dynamics**,** the complex reactions and the formation of reactive species in the gas phase and liquid phase region, and provide beneficial instructions for further process engineering and optimization. Plasma sources (for efficient and selectable production of reactive species in gas phase and subsequently in liquid phase) need to be tailor-made to meet the specific applications. This will be an important work before large-scale industrial applications.

Acknowledgments This work was supported jointly by the National Natural Science Foundation of China under Grant Nos. 51877208, 51777206, and 51807046, Anhui Provincial Key R&D Programmes 202004a07020047, Natural Science Foundation of Anhui Province Grant Nos. 1808085MA13 and 1908085MA29, as well as National Key R&D Program of China with Grant No. 2019YFC0119000.

References

Bae SC, Park SY, Choe W et al (2015) Inactivation of murine norovirus-1 and hepatitis a virus on fresh meats by atmospheric pressure plasma jets. Food Res Int 76:342–347

Barletta F, Leys S, Colombo V et al (2020) Insights into plasma-assisted polymerization at atmospheric pressure by spectroscopic diagnostics. Plasma Process Polym 17:1900174. (15pp)

Benedikt J (2010) Plasma-chemical reactions: low pressure acetylene plasmas. J Phys D Appl Phys 43:043001. (21pp)

Benedikt J, Hofmann s, Knake N, et al. (2010) Phase resolved optical emission spectroscopy of coaxial microplasma jet operated with He and Ar. Eur Phys J D 60:539–546

Berthomieu C, Hienerwadel R (2009) Fourier transform infrared (FTIR) spectroscopy. Photosynth Res 101:157–170

Bieiski BH, Cabelli DE, Arudi RL et al (1985) Reactivity of HO_2/O_2^- radicals in aqueous solution. J Phys Chem Ref Data Monogr 14:1041–1100

Bradford KJ, Dahal P, Van AJ et al (2018) The dry chain: reducing postharvest losses and improving food safety in humid climates. Trends Food Sci Technol 71:84–93

Braithwaite NSTJ (2000) Introduction to gas discharges. Plasma Sources Sci Technol 9:517–527

Bruggeman P, Brandenburg R (2013) Atmospheric pressure discharge filaments and microplasmas: physics, chemistry and diagnostics. J Phys D Appl Phys 46:464001. (28pp)

Bruggeman PJ, Kushner MJ, Locke BR et al (2016) Plasma–liquid interactions: a review and roadmap. Plasma Sources Sci Technol 25:053002. (59pp)

Chen C, Liu DX, Liu ZC et al (2014) A model of plasma-biofilm and plasma-tissue interactions at ambient pressure. Plasma Chem Plasma Process 34:403–4413

Dai XJ, Corr CS, Ponraj SB (2016) Efficient and selectable production of reactive species using a nanosecond pulsed discharge in gas bubbles in liquid. Plasma Processes Polym 13:306–310

Daily JW (1997) Laser induced fluorescence spectroscopy in flames. Prog Energy Combust Sci 23:133–199

Dorai R, Kushner M (2003) A model for plasma modification of polypropylene using atmospheric pressure discharges. J Phys D Appl Phys 36:666–685

Du CM, Sun YW et al (2008) The Effects of gas composition on active species and byproducts formation in gas-water gliding arc discharge. Plasma Chem Plasma Process 28:523–533

Ehlbeck J, Schnabel U, Polak M et al (2011) Low temperature atmospheric pressure plasma sources for microbial decontamination. J Phys D Appl Phys 44:13002. (33pp)

Ekezie FGC, Sun DW, Cheng JH (2017) A review on recent advances in cold plasma technology for the food industry: current applications and future trends. Trends Food Sci Technol 69:46–58

Fierro A, Moore C, Yee B et al (2018) Three-dimensional kinetic modeling of streamer propagation in a nitrogen/helium gas mixture. Plasma Sources Sci Technol 27:105008. (14pp)

Gaens WV, Bogaerts A (2014) Kinetic modelling for an atmospheric pressure argon plasma jet in humid air. J Phys D Appl Phys 47:079502. (3pp)

Gasanova S (2013) Aqueous-phase electrical discharges: generation, investigation and application for organics removal from water. Dissertation, University of Duisburg-Essen

Georgescu N, Apostol L, Gherendi F (2017) Inactivation of *Salmonella enterica* serovar *Typhimurium* on egg surface, by direct and indirect treatments with cold atmospheric, plasma. Food Control 76:52–61

Gessel AFHV, Alards KMJ, Bruggeman PJ (2013) NO production in an RF plasma jet at atmospheric pressure. J Phys D Appl Phys 46:265202. (10pp)

Gorbanev Y, Deborah OC, Chechik V (2016) Non-thermal plasma in contact with water: the origin of species. Chem A Eur J 22:3496–3505

Gurol C, Ekinci FY, Aslan N et al (2012) Low temperature plasma for decontamination of *E. coli* in milk. Int J Food Microbiol 157:1–5

Hamaguchi S (2013) Chemically reactive species in liquids generated by atmospheric-pressure plasmas and their roles in plasma medicine. AIP Conf Proc 1545:214–222

He J, Zhang YT (2012) Modeling study on the generation of reactive oxygen species in atmospheric radio-frequency helium-oxygen discharges plasma. Process Polym 9:919–928

Hojnik N, Celbar U, Tavcar-kalcher G et al (2017) Mycotoxin decontamination of food: cold atmospheric pressure plasma versus "classic" decontamination. Toxins 9:151

Jasinski M, Mizeraczyk J, Zakrzewski Z et al (2002) CFC-11 destruction by microwave torch generated atmospheric-pressure nitrogen discharge. J Phys D Appl Phys 35:2274–2280

Jiang C, Carter C (2014) Absolute atomic oxygen density measurements for nanosecond-pulsed atmospheric-pressure plasma jets using two-photon absorption laser-induced fluorescence spectroscopy. Plasma Sources Sci Technol 23:065006. (10pp)

Jiang J, Tan Z, Shan C et al (2016) A new study on the penetration of reactive species in their mass transfer processes in water by increasing the electron energy in plasmas. Phys Plasmas 23:103503. (10pp)

Jiang JK, Luo YC, Moldgy A et al (2020) Absolute spatially and time-resolved O,O_3, and air densities in the effluent of a modulated RF-driven atmospheric pressure plasma jet obtained by molecular beam mass spectrometry. Plasma Process Polym 17:1900163–1900176

Jimenez-sanchez C, Lozano-sanchez J, Segrua-carretero A et al (2017) Alternatives to conventional thermal treatments in fruit-juice processing. Part 1: techniques and applications. Crit Rev Food Sci Nutr 57:501–523

Jovicevic S, Ivkovic M, Pavlovic Z et al (2000) Parametric study of an atmospheric pressure microwave-induced plasma of the mini MIP torch-I. Two-dimensional spatially resolved electron-number density measurements. Spectrochim Acta Part B 55:1879–1893

Jun-Seok O, Yolanda A-G, James WB (2011) Time-resolved mass spectroscopic studies of an atmospheric-pressure helium microplasma jet. J Phys D Appl Phys 44:365202. (10pp)

Kanazawa S, Kawano H, Watanabe S et al (2011) Observation of OH radicals produced by pulsed discharges on the surface of a liquid. Plasma Sources Sci Technol 20:0340108. (8pp)

Khlyustova A, Labay C, Machala Z et al (2019) Important parameters in plasma jets for the production of RONS in liquids for plasma medicine: a brief review. Front Chem Sci Eng 2:238–252

Kim GJ, Iza F, Lee JK (2006) Electron and ion kinetics in a microhollow cathode discharge. J Phys D Appl Phys 39:4386–4392

Koen VL, Annemie B (2017) Influence of the gap size and dielectric constant of the packing on the plasma discharge in a packed bed dielectric barrier discharge reactor: a fluid modeling study. Plasma Process Polym 14:600129. (11pp)

Kwon HC, Jung SY, Kim HY et al (2014) Abnormal electron-heating mode and formation of secondary-energetic electrons in pulsed microwave-frequency atmospheric microplasmas. Phys Plasmas 21:033511. (7pp)

Lacombe A, Niemira BA, Gurtler JB et al (2015) Atmospheric cold plasma inactivation of aerobic microorganisms on blueberries and effects on quality attributes. Food Microbiol 46:479–484

Laroussi M, Lu XP, Keidar M (2017) Perspective: the physics, diagnostics, and applications of atmospheric pressure low temperature plasma sources used in plasma medicine. J Appl Phys 122:020901. (19pp)

Lee C, Lieberman MA (1995) Global model of Ar, O_2, Cl_2, and Ar/O_2 high-density plasma discharges. J Vac Sci Technol A 13:368–380

Lee HW, Lee HW, Kang SK et al (2013) Synergistic sterilization effect of microwave-excited nonthermal Ar plasma, H_2O_2, H_2O and TiO_2, and a global modeling of the interactions. Plasma Sources Sci Technol 22:055008. (15pp)

Lee MU, Lee JK, Yun GS (2018) Generation of energetic electrons in pulsed microwave plasmas. Plasma Processes Polym 15:1700124. (9pp)

Li D, Nikiforov A, Britun N et al (2016) OH radical production in an atmospheric pressure surface micro-discharge array. J Phys D Appl Phys 49:455202. (12pp)

Liao XY, Liu DH, Xiang QS et al (2017) Inactivation mechanisms of non-thermal plasma on microbes: a review. Food Control 75:83–91

Lieberman MA, Lichtenberg AJ (1994) Principles of plasma discharges and materials processing. John Wiley & Sons, Inc., New York

Lietz AM, Kushner M (2018) Molecular admixtures and impurities in atmospheric pressure plasma jets. J Appl Phys 124:153303. (15pp)

Liu DX, Bruggeman P, Iza F et al (2010) Global model of low-temperature atmospheric-pressure He+H_2O plasmas. Plasma Sources Sci Technol 19:025018. (2pp)

Liu DX, Iza F, Wang XH et al (2011) He+O_2+H_2O plasmas as a source of reactive oxygen species. Appl Phys Lett 98:221501. (3pp)

Liu YF, Liu DX, Zhang JS et al (2020) 1D fluid model of RF-excited cold atmospheric plasmas in helium with air gas impurities. Phys Plasmas 27:04351. (16pp)

Lu XP, Jiang ZH, Xiong Q et al (2008) An 11 cm long atmospheric pressure cold plasma plume for applications of plasma medicine. Appl Phys Lett 92:081502. (2pp)

Lu XP, Laroussi M, Puech V (2012) On atmospheric-pressure non-equilibrium plasma jets and plasma bullets. Plasma Sources Sci Technol 21:034005. (17pp)

Lu XP, Naidis GV, Laroussi M et al (2016a) Reactive species in non-equilibrium atmospheric-pressure plasmas: generation, transport, and biological effects. Phys Rep 630:1–84

Lu XP, Cullen PJ , Ostrikov K (2016b) Atmospheric pressure nonthermal plasma sources. In: Misra NN, Oliver S, Cullen PJ (eds) Cold plasma in food and agriculture. Academic Press, London, pp 83–116

Lu P, Boehm D, Bourke P et al (2017) Achieving reactive species specificity within plasma-activated water through selective generation using air spark and glow discharges. Plasma Processes Polym 14:e1600207. (9pp)

Lukes P, Locke BR (2005) Plasma chemical oxidation processes in a hybrid gas-liquid electrical discharge reactor. J Phys D Appl Phys 38:4074–4081

Lukes P, Dolezalova E, Sisrova I et al (2014) Aqueous-phase chemistry and bactericidal effects from an air discharge plasma in contact with water: evidence for the formation of peroxynitrite through a pseudo-second-order post-discharge reaction of H_2O_2 and HNO_2. Plasma Sources Sci Technol 23:015019. (15pp)

Ma RN, Wang GM, Tian Y et al (2015) Non-thermal plasma-activated water inactivation of food-borne pathogen on fresh produce. J Hazard Mater 300:643–651
Machala Z, Tarabova B, Hensel K et al (2013) Formation of ROS and RNS in water electro-sprayed through transient spark discharge in air and their bactericidal effects. Plasma Processes Polym 10:649–659
Marskar R (2020) 3D fluid modeling of positive streamer discharges in air with stochastic photoionization. Plasma Sources Sci Technol 29:055007. (11pp)
Mir SA, Shah MA, Mir MM (2016) Understanding the role of plasma technology in food industry. Food Bioproc Tech 9:734–750
Misra NN, Tiwari BK, Raghavarao, et al. (2011) Nonthermal plasma inactivation of food-borne pathogens. Food Eng Rev 3:159–170
Murakami T, Niemi K, Gans T et al (2013) Chemical kinetics and reactive species in atmospheric pressure helium-oxygen plasmas with humid-air impurities. Plasma Sources Sci Technol 22:015003. (29pp)
Murray K, Wu F, Shi J et al (2017) Challenges in the microbiological food safety of fresh produce: limitations of post-harvest washing and the need for alternative interventions. Food Qual Saf 1:289–301
Nguyen DB, Mok YS, Lee WG (2019) Enhanced atmospheric pressure plasma jet performance by an alternative dielectric barrier discharge configuration. IEEE Trans Plasma Sci 47:4795–4801
Nikiforov A, Sarani A, Leys C (2011) The influence of water vapor content on electrical and spectral properties of an atmospheric pressure plasma jet. Plasma Sources Sci Technol 20:15014–15021
Niquet R, Boehm D, Schnabel U (2018) Characterising the impact of post-treatment storage on chemistry and antimicrobial properties of plasma treated water derived from microwave and DBD sources. Plasma Process Polym 15:e1700127. (11pp)
Pan YY, Cheng JH, Sun DW (2019) Cold plasma-mediated treatments for shelf life extension of fresh produce: a review of recent research developments. Compr Rev Food Sci Food Saf 18:1312–1326
Pankaj SK, Bueno-ferrer C, Misra NN, et al. (2014). Applications of cold plasma technology in food packaging. Trends in Food Science & Technology, 35: 5-17
Park GY, Park SJ, Choi MY (2012) Atmospheric-pressure plasma sources for biomedical applications. Plasma Sources Sci Technol 21:043001. (21pp)
Pavlovich MJ, Chang HW, Sakiyama Y et al (2013) Ozone correlates with antibacterial effects from indirect air dielectric barrier discharge treatment of water. J Phys D Appl Phys 46:145202. (10pp)
Rees JA, Seymour DL, Greenwood C-L et al (2010) Mass and energy spectrometry of atmospheric pressure plasmas. Plasma Processes Polym 7:92–101
Reuter S, Woedtke TV, Weltmann KD (2018) The kINPen-a review on physics and chemistry of the atmospheric pressure plasma jet and its applications. J Phys D Appl Phys 51:233001. (51pp)
Roy NC, Hasan HH, Kabir AH et al (2018) Atmospheric pressure gliding arc discharge plasma treatments for improving germination, growth and yield of wheat. Plasma Sci Technol 20:115501. (11pp)
Sarangapani C, Misra NN, Milosavljevic V et al (2016) Pesticide degradation in water using atmospheric air cold plasma. J Water Process Eng 9:225–232
Sato Y, Ishikawa K, Tsutsumi T et al (2020) Numerical simulations of stable, high-electron-density atmospheric pressure argon plasma under pin-to-plane electrode geometry: effects of applied voltage polarity. J Phys D Appl Phys 53:265204. (14pp)
Schroter S, Wijaikhum A, Gibson AR (2018) Chemical kinetics in an atmospheric pressure helium plasma containing humidity. Phys Chem Chem Phys 20:24263–24,286
Shen J, Sun Q, Zhang ZL et al (2015) Characteristics of DC gas-liquid phase atmospheric-pressure plasma and bacteria inactivation mechanism. Plasma Processes Polym 12:252–259
Shen J, Zhang H, Xu ZM et al (2019) Preferential production of reactive species and bactericidal efficacy of gas-liquid plasma discharge. Chem Eng J 362:402–412

Sousa JS, Puech V (2013) Diagnostics of reactive oxygen species produced by microplasmas. J Phys D Appl Phys 46:464005. (12pp)
Stephens J, Abide M, Fierro A, Neuber A (2018) Practical considerations for modeling streamer discharges in air with radiation transport. Plasma Sources Sci Technol 27:075007. (9pp)
Stoffels E, Gonzalvo YA, Whitmore TD et al (2007) Mass spectrometric detection of short-living radicals produced by a plasma needle. Plasma Sources Sci Technol 16:549–556
Suhem K, Matan N, Nisoa M et al (2013) Inhibition of *Aspergillus flavus* on agar media and brown rice cereal bars using cold atmospheric plasma treatment. Int J Food Microbiol 2013:107–111
Sun B, Liu DX, Iza F et al (2019a) Global model of an atmospheric-pressure capacitive discharge in helium with air impurities from 100 to 10,000 ppm. Plasma Sources Sci Technol 28:035006. (22pp)
Sun B, Liu DX, Wang XH (2019b) Reactive species in cold atmospheric-pressure He+Air plasmas: the influence of humidity. Phys Plasmas 26:063514. (13pp)
Surowsky B, Schluter O, Knorr D (2015) Interactions of non-thermal atmospheric pressure plasma with solid and liquid food systems: a review. Food Eng Rev 7:82–108
Tani A, Ono Y, Fukui S et al (2012) Free radicals induced in aqueous solution by non-contact atmospheric-pressure cold plasma. Appl Phys Lett 100:254103. (3pp)
Tavant A, Lieberman MA (2016) Hybrid global model of water cluster ions in atmospheric pressure Ar/H_2O RF capacitive discharges. J Phys D Appl Phys 49:465201
Teunissen J, Ebert U (2016) 3D PIC-MCC simulations of discharge inception around a sharp anode in nitrogen/oxygen mixtures. Plasma Sources Sci Technol 25:044005. (13pp)
Tian W, Kushner MJ (2014) Atmospheric pressure dielectric barrier discharges interacting with liquid covered tissue. J Phys D Appl Phys 47:165201. (21pp)
Torres J, Palomares JM, Sola A et al (2007) A Stark broadening method to determine simultaneously the electron temperature and density in high-pressure microwave plasmas. J Phys D Appl Phys 40:5929–5936
Uchida G, Nakajima A, Ito T et al (2016) Effects of nonthermal plasma jet irradiation on the selective production of H_2O_2 and NO_2^- in liquid water. J Appl Phys 120:203302. (9pp)
Uhm HS, Hong YC, Shin DH (2006) A microwave plasma torch and its applications. Plasma Sources Sci Technol 15:S26–S34
Von WT, Oehmigen K, Brandenburg R et al (2012) Plasma-liquid interactions: chemistry and antimicrobial effects. In: Plasma for bio-decontamination medicine and food security. Springer, Netherlands, pp 67–78
Wagner HE, Brandenburga R, Kozlovb KV (2003) The barrier discharge: basic properties and applications to surface treatment. Vacuum 71:417–436
Walsh JL, Kong MG (2008) Contrasting characteristics of linear-field and cross-field atmospheric plasma jets. Appl Phys Lett 93:111501. (3pp)
Wang ZH, Ma WH, Chen CC et al (2011) Probing paramagnetic species in titania-based heterogeneous photocatalysis by electron spin resonance (ESR) spectroscopy-A mini review. Chem Eng J 170:353–362
Wang G, Kuang Y, Zhang YT (2020) Kinetic simulation of the transition from a pulse-modulation microwave discharge to a continuous plasma. Plasma Sci Technol 22:015404. (8pp)
Waskoenig J, Niemi K, Knake N et al (2010) Atomic oxygen formation in a radio-frequency driven micro-atmospheric pressure plasma jet. Plasma Sources Sci Technol 19:045018. (11pp)
Weltmann K-D, Woedtke TV (2017) Plasma medicine-current state of research and medical application. Plasma Phys Control Fusion 59:014031. (11pp)
Winter J, Brandenburg R, Weltmann K-D (2015) Atmospheric pressure plasma jets: an overview of devices and new directions. Plasma Sources Sci Technol 24:064001. (19pp)
Wu AJ, Zhang H, Li XD et al (2015) Determination of spectroscopic temperatures and electron density in rotating gliding arc discharge. IEEE Trans Plasma Sci 43:836–845
Yan DY, Jonathan HS, Keidar M (2017) Cold atmospheric plasma, a novel promising anti-cancer treatment modality. Oncotarget 8:15977–15995

Yang AJ, Liu DX, Rong MZ et al (2014) A dominant role of oxygen additive on cold atmospheric-pressure He + O_2 plasmas. Phys Plasmas 21:083501. (6pp)
Zahoranova A, Henselova M, Hudecova D et al (2016) Effect of cold atmospheric pressure plasma on the wheat seedlings vigor and on the inactivation of microorganisms on the seeds surface. Plasma Chem Plasma Process 36:397–414
Zhang, ZL, Xu, ZM, Cheng,C, et al. (2017). Bactericidal effects of plasma induced reactive species in dielectric barrier gas-liquid discharge, Plasma Chem Plasma Process, 37: 415–431.
Zhou R, Zhou R, Prasad K et al (2018) Cold atmospheric plasma activated water as a prospective disinfectant: the crucial role of peroxynitrite. Green Chem 20:5276–5284
Zhu XM, Chen WC, Pu YK (2008) Gas temperature, electron density and electron temperature measurement in a microwave excited microplasma. J Phys D Appl Phys 41:105212. (6pp)
Zhu FS, Zhang H, Li XD et al (2018) Arc dynamics of a pulsed DC nitrogen rotating gliding arc discharge. J Phys D Appl Phys 51:105202. (8pp)